EGF induces coalescence of different lipid rafts

Erik G. Hofman[1], Mika O. Ruonala[2], Arjen N. Bader[3], Dave van den Heuvel[3], Jarno Voortman[1], Rob C. Roovers[1], Arie J. Verkleij[1], Hans C. Gerritsen[3] and Paul M. P. van Bergen en Henegouwen[1,*]

[1]Department of Cellular Architecture and Dynamics, Institute of Biomembranes, Utrecht University, Utrecht, The Netherlands
[2]Center for Membrane Proteomics, University of Frankfurt, Biocenter, Frankfurt am Main, Germany
[3]Department of Molecular Biophysics, Utrecht University, Utrecht, The Netherlands
*Author for correspondence (e-mail: p.vanbergen@uu.nl)

Accepted 19 May 2008
Journal of Cell Science 121, 2519-2528 Published by The Company of Biologists 2008
doi:10.1242/jcs.028753

Summary

The suggestion that microdomains may function as signaling platforms arose from the presence of growth factor receptors, such as the EGFR, in biochemically isolated lipid raft fractions. To investigate the role of EGFR activation in the organization of lipid rafts we have performed FLIM analyses using putative lipid raft markers such as ganglioside GM1 and glycosylphosphatidylinositol (GPI)-anchored GFP (GPI-GFP). The EGFR was labeled using single domain antibodies from *Llama glama* that specifically bind the EGFR without stimulating its kinase activity. Our FLIM analyses demonstrate a cholesterol-independent colocalization of GM1 with EGFR, which was not observed for the transferrin receptor. By contrast, a cholesterol-dependent colocalization was observed for GM1 with GPI-GFP. In the resting state no colocalization was observed between EGFR and GPI-GFP, but stimulation of the cell with EGF resulted in the colocalization at the nanoscale level of EGFR and GPI-GFP. Moreover, EGF induced the enrichment of GPI-GFP in a detergent-free lipid raft fraction. Our results suggest that EGF induces the coalescence of the two types of GM1-containing microdomains that might lead to the formation of signaling platforms.

Supplementary material available online at
http://jcs.biologists.org/cgi/content/full/121/15/2519/DC1

Key words: EGFR, FRET/FLIM, GM1, GPI-GFP, Lipid raft

Introduction

Lateral membrane heterogeneity has been generally accepted as a requirement for correct functioning of biological membranes (for reviews see Jacobson et al., 2007; Mayor and Rao, 2004; Pike, 2004). Within this concept, lipid rafts have been proposed to represent microdomains enriched in cholesterol and sphingolipids such as gangliosides. In response to signaling, lipid rafts may fuse into larger and more stable structures resulting in the formation of efficient signaling platforms (Simons and Toomre, 2000). Three different microdomain concepts have recently been suggested that differ in both size and composition (Jacobson et al., 2007). (1) Small-scale domains or shells composed of a transmembrane protein surrounded by a shell of cholesterol and glycosphingolipids; (2) nanodomains or lipid rafts that represent larger structures composed of cholesterol, glycosphingolipids and additional proteins such as caveolin and; (3) larger microdomains, identified using light-microscopy and single-molecule imaging, which contain both proteins and lipids that are limited in their free mobility by the membrane skeleton (Kusumi et al., 2004).

The epidermal growth factor receptor (EGFR) was one of the first examples of a lipid-raft-localized growth factor receptor (Mineo et al., 1996; Pike, 2005). The EGFR is a member of the ErbB family of receptor tyrosine kinases, consisting of an ectodomain composed of two ligand-binding domains and two cysteine-rich domains, a transmembrane stretch, and an intracellular tyrosine kinase domain connected to a tyrosine-rich substrate region (Jorissen et al., 2003). Binding of EGF to the ligand-binding sites induces a conformational change in the ectodomain that enables receptor dimerization, which in turn leads to cross-phosphorylation of intracellular tyrosine residues and docking of SH2-domain or PTB-domain-containing adaptor and/or effector proteins (Dawson et al., 2007). Mutational analysis has revealed sequences in the second cysteine-rich domain of the EGFR ectodomain that are required for their co-fractionation with detergent-free lipid raft fractions (Yamabhai and Anderson, 2002). Immunogold electron microscopy showed that a substantial amount of the EGFR is located in rafts but not in caveolae, supporting the hypothesis for the coexistence of different kinds of microdomains (Ringerike et al., 2002). Stimulation of EGFR signaling induces the internalization through GM1-enriched vesicles that endocytose using both clathrin-dependent and clathrin-independent mechanisms (Puri et al., 2005; Sigismund et al., 2005). Indications for the presence of the EGFR in microdomains have been obtained using single-molecule imaging of the EGFR (Orr et al., 2005). The mobility of the EGFR in those microdomains was shown to be dependent upon cholesterol and the cytoskeleton.

Localization of the EGFR in lipid rafts has been suggested to have an effect on the two principal functions of the EGFR: ligand binding and tyrosine kinase activity. Interestingly, opposing effects have been obtained for the typical raft lipids on receptor functioning. Enhanced EGF-binding to EGFR was observed when cholesterol and phosphatidylinositol (PdtIns) were added to dioleoyl-phosphatidylcholine (DOPC) liposomes in which the EGFR was reconstituted (den Hartigh et al., 1993). Conversely, extraction of cholesterol from cells was shown to increase EGF-binding and to stimulate ligand-independent EGFR tyrosine-kinase activity and subsequent signaling to ERK1 and ERK2 (ERK1/2) (Furuchi and Anderson, 1998; Pike and Casey, 2002; Roepstorff et al., 2002). Also, gangliosides were shown to alter the phosphorylation state of the EGFR (Miljan and Bremer, 2002). Although some gangliosides, such as GM3, have been published to inhibit EGF-induced phosphorylation of the receptor (Bremer et al., 1984; Miljan and Bremer, 2002), other gangliosides, such as GM1 or GD1a, have

Journal of Cell Science

been reported to enhance EGFR phosphorylation in response to EGF (Li et al., 2001; Liu et al., 2004; Miljan et al., 2002). Moreover, cells with excess GD3 gangliosides were found to have decreased EGFR phosphorylation levels, whereas overexpression of enzymes required for GM1 synthesis resulted in enhanced cell proliferation in response to EGF (Nishio et al., 2005; Zurita et al., 2001). Although the lipid composition of the membrane in which the EGFR is embedded appears to be an important regulator of the EGFR (Miljan and Bremer, 2002), the molecular mechanisms as to how these lipids regulate the EGFR functionality are far from clear.

A popular approach to study the functionality of lipid rafts has been their biochemical isolation. Co-fractionation of the EGFR with the detergent-resistant membrane (DRM) fraction strongly depends on the applied purification method (Pike, 2004). EGFR is absent from the DRM fraction when the standard non-ionic detergent Triton X-100 was used, but detergent-resistant fractions prepared with Brij 98 or Lubrol, or the detergent-free floating fractions usually contain EGFR (Pike, 2004). Also, in the DRM fraction obtained from carbonate-treated cells, the EGFR is detectable (Mineo et al., 1996). Thus, co-fractionation of proteins with the DRM fraction does not necessarily imply that such components are present in lipid rafts in the cell membrane (Lichtenberg et al., 2005).

To study the presence and functioning of the EGFR in lipid rafts in the context of the plasma membrane, non-invasive techniques such as fluorescence microscopy are required (Lagerholm et al., 2005; Rao and Mayor, 2005). Unfortunately, the resolution power of standard fluorescence microscopy (~200 nm) does not permit a direct visualization of lipid rafts of an estimated size of 1-100 nm. Logically, direct verification of the presence of the EGFR in lipid rafts is equally excluded. Förster resonance energy transfer (FRET) imaging (Jares-Erijman and Jovin, 2006) reports for the intramolecular distance between two fluorescent molecules at nanometer scale (1-10 nm). Thus, FRET can be used to determine the close proximity and colocalization of two molecules. In our work presented here, the colocalization of the EGFR with molecules that are typically present in DRM fractions, such as the ganglioside GM1 and glycosylphosphatidylinositol-anchored GFP (GPI-GFP), is studied by making use of FRET imaging. Here, two levels of colocalization are considered, (1) *microscopic scale* colocalization on a pixel level and (2) *nanoscale* colocalization as determined using FRET. To label the EGFR without changing its activity state we have used monovalent, non-agonistic fragments from heavy-chain only antibodies from *Llama glama* (nanobodies^{TM}), which were directed against the ectodomain of the EGFR. Ganglioside GM1 was labeled using subunit B from cholera toxin (CTB). To circumvent effects the probe concentration might have on energy transfer, we investigated the occurrence of FRET by time-gated fluorescent lifetime imaging microscopy (FLIM). We report here the cholesterol-independent colocalization of GM1 with EGFR, whereas the colocalization of GM1 with GPI-GFP is cholesterol-dependent. No colocalization of GM1 was observed with the transferrin receptor (TfR), demonstrating the selectivity of the assay. Stimulation of the cells with EGF induced EGFR colocalization with GPI-GFP. Our results suggest that the EGFR is surrounded by gangliosides and that EGF stimulation leads to coalescence of different types of lipid raft into larger EGFR-containing lipid nanodomains.

Results

Development of nanobodies against EGFR

To investigate the localization of the EGF receptor in the plasma membrane, small, monovalent and highly specific probes that do not induce EGFR activation or internalization are required. To this end, we decided to use antibodies from *Llama glama* that are devoid of light chains and, as such, only consists of heavy chains (Conrath et al., 2003). The variable part of the heavy chain of these heavy-chain-only antibodies (termed VHH) fulfils all the above described criteria. Because of their small size (~15 kDa) we refer to this antibody format as nanobody.

A VHH immune library directed against EGFR was produced as previously described (Roovers et al., 2007). From this library, three different nanobodies were selected and further characterized

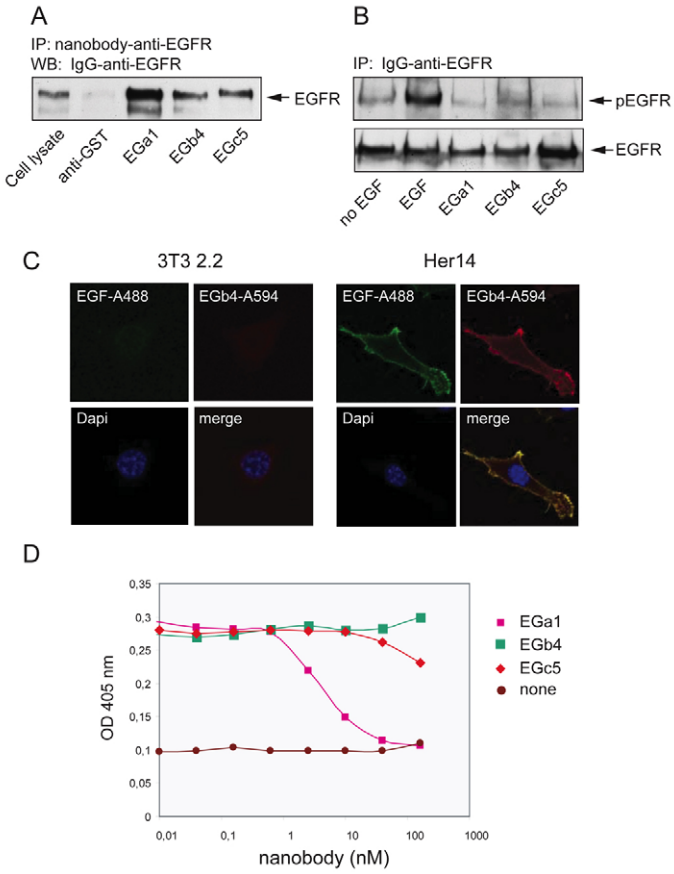

Fig. 1. Characterization of anti-EGFR nanobodies. (A) Immunoprecipitation of EGFR with nanobodies. HER14 cell lysates were prepared as described in Material and Methods and incubated for 1 hour at 4°C with Talon beads preloaded with the indicated anti-EGFR nanobodies, or with an non-specific nanobody (anti-GST). Bound proteins were separated by SDS-PAGE, analyzed by western blotting. Control lane (Cell lysate) is loaded with 10% of the lysate. (B) Selected nanobodies are non-agonistic. An equal number of serum-depleted HER14 cells was treated with either 8 nM EGF, 1 μM of the indicated nanobodies for 10 minutes, or mock-treated (no EGF), and immunoprecipitated EGFR was analyzed by western blotting. Activation of EGFR was determined with an antibody against phosphorylated tyrosine at position 1068 (pEGFR). Loading control was performed with anti-EGFR (EGFR). (C) Selected nanobodies bind specifically to EGFR. NIH 3T3 clone 2.2 cells, lacking detectable expression of EGFR, or HER14 cells were labeled at 4°C for 60 minutes with 100 nM EGb4-A594. In parallel, the cells were labeled with 8 nM EGF-A488 and nuclei were visualized with 4′-6-diamidino-2-phenylindole (DAPI; blue). (D) Different antagonistic activities of anti-EGFR nanobodies. HER14 cells grown in 96-well plates, were pre-incubated with biotinylated EGF, followed by increasing concentrations of indicated nanobodies or EGF. Binding of EGF-biotin on the cell surface was quantified using peroxidase-conjugated streptavidin, followed by addition of the substrate OPD.

for EGFR-binding specificity and biological activity. Binding to EGFR was analyzed by immunoprecipitation, and all three selected nanobodies were found to bind EGFR, as demonstrated by the immunoprecipitation of EGFR from the cell lysate (Fig. 1A). As a control, Talon® beads were preloaded with nanobodies directed against glutathione-S-transferase (anti-GST) that did not precipitate EGFR. Biological activity of the nanobodies was checked by analysing EGFR activation using antibodies against the phosphorylated C-terminal domain of EGFR. HER14 cells (mouse NIH 3T3 fibroblasts expressing human EGFR) were incubated for 10 minutes with 1 μM nanobody or 8 nM EGF, and immunoprecipitates of EGFR from the cell lysate were analyzed by western blotting with anti-phosphotyrosine1068-EGFR or anti-EGFR as loading control. A clear EGF-mediated activation of EGFR was found, but no EGFR activation could be detected after incubation with the different nanobodies, although their concentration exceeded EGF concentration 125 times (Fig. 1B). To check the specificity of the nanobodies for EGFR, we incubated NIH 3T3 clone 2.2 cells, which have no detectable levels of EGFR, and HER14 cells on ice with 100 nM anti-EGFR nanobody directly conjugated to Alexa-Fluor-594 (EGb4-A594), in the presence of 8 nM EGF-A488. Nuclear staining with DAPI was used as counter stain. The NIH 3T3 clone 2.2 cells lacking EGFR expression displayed no cell-surface labeling of anti-EGFR nanobodies, whereas HER14 cells were heavily labeled by both probes (Fig. 1C). Moreover, the two probes colocalized exactly, indicating that the nanobody is specific for EGFR. Similar results were obtained with the nanobody EGbc5 (data not shown).

To examine the effect of the nanobodies on EGF binding, we performed a competition assay with biotinylated EGF as previously described (Roovers et al., 2007). Nanobody EGa1 at 1 nM or higher clearly competed with EGF, whereas EGb4 had no effect on EGF binding within the tested concentration range. Only nanobody EGc5 has a minor antagonistic effect above 50 nM (Fig. 1D). In conclusion, we have selected different anti-EGFR nanobodies without detectable agonistic effects on the receptor. One of the nanobodies can block the binding of EGF to the EGFR, whereas the other nanobodies hardly display any blocking capacity, suggesting differential epitope specificity. In addition, conjugation of the nanobodies to Alexa-Fluor probes did not interfere with their binding properties, making these molecules ideal probes for the localization of EGFR in the plasma membrane.

Colocalization of EGFR with GM1 but not with GPI-GFP

The labeled, EGFR-specific nanobodies were used to investigate the colocalization of EGFR with GM1. HER14 cells were labeled with EGa1 conjugated to A488 (EGa1-A488) and the B-subunit of cholera toxin conjugated to A594 (CTB-A594). On the light microscopy level, clear colocalization of the probes over the cell membrane is observed, in particular at membrane ruffles (supplementary material Fig. S1, top row). The average lifetime of donor EGa1-A488 was determined in the absence and presence of acceptor CTB-A594 (Fig. 2A). The lifetime of EGa1-A488 was significantly reduced in the presence of CTB-A594, indicating that EGFR and GM1 are present in the plasma membrane within the range of FRET to occur. To exclude a possible nanobody specific effect, we also used other anti-EGFR nanobodies, such as EGb4, with similar results (Fig. 2B). To exclude a possible crosslinking effect of the formaldehyde fixation, the colocalization of EGFR with GM1 was also studied using live cell frequency-domain FLIM setup – with similar results (M.O.R. and Philippe Bastiaens, unpublished observations). As a negative control, we conducted a colocalization experiment using TfR, which has been found in cell fractionation studies in the detergent-soluble fraction (Harder et al., 1998; Puri

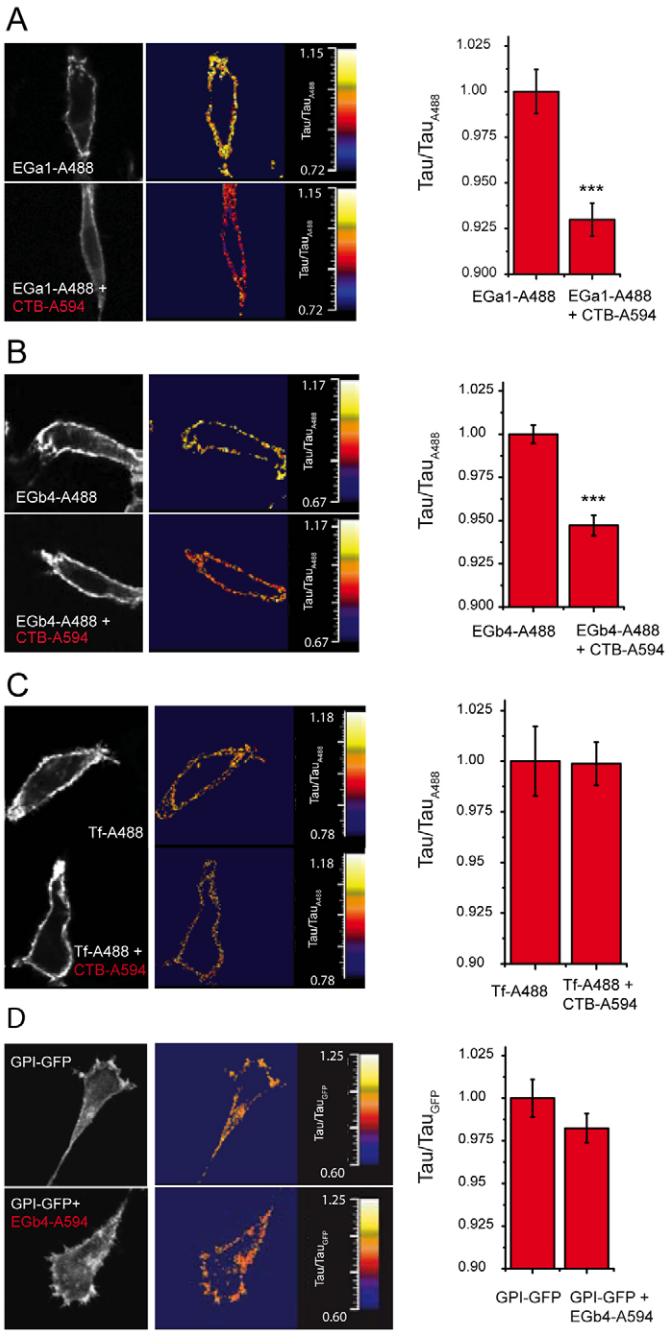

Fig. 2. Nanoscale colocalization of EGFR with GM1 gangliosides. (A-C) HER14 cells grown on coverslips were incubated on ice with 100 nM (A) of the donor probes anti-EGFR nanobody EGa1 or (B) EGb4 directly conjugated to Alexa-Fluor-488, or with (C) 20 μg/ml transferrin-A488 (Tf-A488) in the absence or presence of 1 μg/ml of the acceptor probe CTB-A594. (D) HER14 cells expressing GPI-GFP were incubated or not for 1 hour on ice with 100 nM EGb4-A594 (acceptor). After fixation with 4% formaldehyde, average lifetime values of GFP were determined as described in Materials and Methods. Left panels represent the distributions of the donor probes with or without acceptor probe. The lifetimes are shown in the middle panels in false colors. Mean fluorescent lifetime values ± s.e.m. (***P<0.0001) are presented in histograms on the right.

et al., 2005). This control is particularly important because CTB might – as a result of its pentavalency – induce clustering of GM1, resulting in the recruitment of plasma membrane receptors into these GM1 clusters (Zhang et al., 1995). HER14 cells that transiently express human TfR were fluorescently labeled with transferrin-A488 (Tf-A488). TfR labeling resulted in a heterogenous staining of the cell membrane with a clear microscale colocalization with CTB (supplementary material Fig. S1, bottom row). The lifetime of Tf-A488 remained unaffected when measured in combination with CTB-A594 (Fig. 2C), excluding colocalization of TfR with GM1 on the nanoscale level.

We subsequently investigated whether GPI-GFP colocalizes with EGFR. The GPI-GFP was ectopically expressed in HER14 cells and was found in the plasma membrane, as well as in subcellular compartments (supplementary material Fig. S2, top row). Co-staining with the Golgi-resident protein GM130 identified this compartment as the Golgi complex (supplementary material Fig. S2, bottom row). Confocal images showed a clear colocalization of EGFR with GPI-GFP (supplementary material Fig. S2). However, this colocalization was not confirmed at the nanoscale level by FLIM-analysis. Although a slight lifetime reduction was observed in the presence of EGb4-A594, this difference appeared not to be significant (Fig. 2D). These results demonstrate that EGFR and GPI-GFP do not colocalize in nonstimulated HER14 cells.

In summary, our results demonstrate that the EGFR colocalizes at a nanoscale level with the ganglioside GM1 in the plasma membrane of HER14 cells; for the control receptor TrfR, however, no colocalization was observed. Similarly, colocalization at the nanoscale level for EGFR with GPI-GFP, another frequently used lipid raft marker, was also absent. In addition, the microscopic colocalization of TfR with GM1 and EGFR with GPI-GFP is not detected on a nanoscale using FLIM, demonstrating the power of FRET/FLIM analysis for reliable conclusions on colocalization experiments.

Nanoscale colocalization of GM1 with EGFR is cholesterol independent

We next investigated the role of cholesterol in the colocalization of EGFR with the different markers. For these experiments we used the polyene antibiotic nystatin, which sequesters free cholesterol without considerable extraction of this sterol (Foster et al., 2003). Since another cholesterol-extracting agent, methyl-β-cyclodextrin, has previously been found to stimulate EGFR activity, we checked the effect of nystatin on several cellular functions (Lambert et al., 2006; Ringerike et al., 2002). These control experiments showed that nystatin treatment did not affect EGFR activity, cell shape, or the distribution of GM1, GPI-GFP or EGFR (supplementary material Figs S3 and S4).

We next analyzed the effect of nystatin on the distribution of the two raft markers GPI-GFP and GM1. GPI-GFP was found at the plasma membrane and in the Golgi complex (supplementary material Fig. S3). A clear lifetime reduction of GPI-GFP was observed when the cells were labeled together with CTB-A594 (Fig. 3A). As expected, the false-color images reveal that this lifetime reduction is only found at the plasma membrane, whereas it remained unchanged in intracellular compartments (Golgi) (Fig. 3A). In parallel, GPI-GFP-expressing cells were preincubated with nystatin for 30 minutes, followed by staining with CTB-A594. However, whereas in control cells the lifetime of GPI-GFP was clearly reduced after the addition of CTB-A594, the lifetime of GPI-GFP was not reduced by CTB-A594 in the presence of nystatin (Fig. 3A). This result demonstrates that the two raft markers GM1 and GPI-GFP colocalize in a cholesterol-dependent fashion, which is in agreement with current models of lipid rafts (Kenworthy et al., 2000).

We subsequently studied the effect of nystatin on the colocalization of GM1 with EGFR. HER14 cells were preincubated with nystatin under similar experimental conditions as described above, and labeled with EGa1-A488 and CTB-A595. Again, on a microscale, no clear differences in the distribution of either of the probes in the presence or absence of nystatin was observed (supplementary material Fig. S4). FRET/FLIM analysis showed that nystatin did not affect the observed FRET between the donor-acceptor pair, indicating that the nanoscale colocalization of EGFR and GM1 is cholesterol independent (Fig. 3B). A slight reduction was observed in the lifetime of the EGa1-probe alone, possibly resulting from EGFR clustering

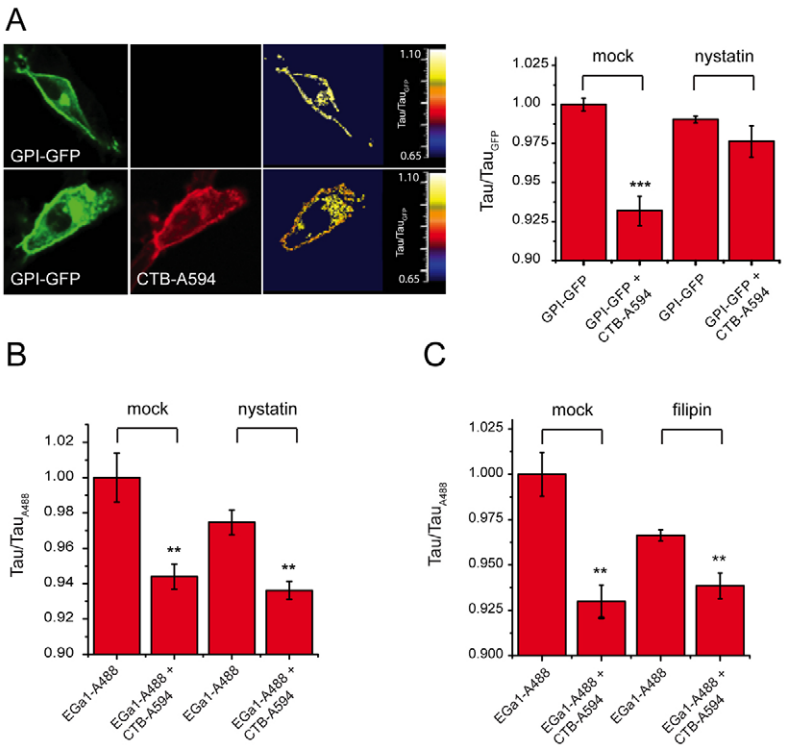

Fig. 3. Cholesterol-dependence of the colocalization of GPI-GFP and EGFR with GM1. (A) Cholesterol-dependent colocalization of GPI-GFP with GM1. HER14 cells expressing GPI-GFP (donor) were incubated or not with 5 μg/ml nystatin for 30 minutes at 37°C and labeled or not with CTB-A594 (donor probe). The fluorescent intensity of GPI-GFP or CTB-A594 is shown in the left or middle panel, respectively. Fluorescent lifetime of GPI-GFP was analyzed as described in Materials and Methods and presented as false-colored images in the right panel. Histograms represent the mean lifetime values ± s.e.m. (***P<0.0001) of GPI-GFP determined under the indicated conditions. (B,C) Cholesterol-independent colocalization EGFR with GM1 gangliosides. HER14 cells were treated with (B) 5 μg/ml nystatin or (C) 2.5 μg/ml filipin for 30 minutes at 37°C. Cells were labeled with anti-EGFR nanobody EGa1-A488 and labeled or not with the acceptor probe CTB-A594. Lifetime values were determined as indicated in Materials and Methods, and mean lifetime values of ± s.e.m. (**P<0.001) are presented in histograms.

as a result of the cholesterol sequestration. Similar results were obtained when the cells were pre-treated with another cholesterol-sequestering agent, filipin (Fig. 3C). In conclusion, our results demonstrate that GM1 and GPI-GFP colocalize in the cell membrane of HER14 cells in a cholesterol-dependent manner. By contrast, the colocalization of GM1 with the EGFR was not affected by the sequestration of cholesterol, demonstrating that the EGFR-GM1 colocalization is cholesterol independent.

EGF induces nanoscale colocalization of EGFR with GPI-GFP

We next analyzed the effect of EGFR signaling on the nanoscale colocalization of the EGFR with the two lipid raft markers. To prevent internalization of the receptor after activation, these experiments were performed at ice-cold conditions. Stimulation with EGF at this temperature was found to result in phosphorylation of the receptor to an extent and with kinetics that were similar to the phosphorylation induced at 37°C (Fig. 4A). These results are in agreement with previous data, showing that EGFR signaling was still able to proceed at 4°C (McCune and Earp, 1989). The effect of EGF stimulation on the colocalization between EGFR and GM1 was first studied using EGF-A488 as donor probe and CTB-A594 as acceptor probe. In this way, EGF-A488 serves both as a donor-probe and as a ligand for EGFR. The presence of the acceptor probe reduced the lifetime of EGF-A488 significantly, indicating that the colocalization of EGFR with GM1 at the nanoscale level still exists after activation of EGFR (Fig. 4B). In an alternative approach, we used the non EGF-competing nanobody EGb4 conjugated to A488 as donor probe. Labeling of HER14 cells with EGb4-A488 was followed by activation of the cells with 8 nM EGF for 10 minutes. In the absence of EGF, a significant lifetime reduction was observed in the presence of CTB-A594, which remained unaltered after treatment of the cell with EGF. The results demonstrate that EGFR activation does not affect colocalization between EGFR and GM1. In addition, EGF was found to induce a slight reduction in the lifetime of the EGb4-A488 probe, possibly a result of the EGF-induced receptor oligomerization.

To measure the effect of EGF on the colocalization of the EGFR with GPI-GFP, HER14 cells stably expressing GPI-GFP were labeled for 1 hour with EGF-Rhodamine, and the lifetime of the donor probe (GPI-GFP) was determined. Interestingly, the lifetime of GPI-GFP was clearly decreased in the presence of EGF-Rhodamine, suggesting that activation of the EGF receptor induces the colocalization of EGFR and GPI-GFP (Fig. 5A). EGF alone did not have an effect on the lifetime of GPI-GFP, indicating that the acceptor probe is required for this effect (Fig. 5B). In an alternative approach, we first labeled EGFR with EGc5-A594, a non-competing anti-EGFR nanobody conjugated to A594. After washing, the cells were stimulated with EGF and analyzed by FLIM. In the non-stimulated cells, no lifetime reduction of GPI-GFP was observed, whereas after 10 minutes of stimulation with EGF a significant lifetime reduction became apparent (Fig. 5B). In parallel, nanobody EGb4 was used in a similar way, as an acceptor probe in combination with GPI-GFP, yielding similar results (data not shown). We finally investigated the role of cholesterol in the EGF-induced colocalization of EGFR and GPI-GFP. Lifetime analysis of EGF-stimulated and nystatin-treated GPI-GFP-expressing cells demonstrated that the nanoscale colocalization of EGFR with GPI-GFP is cholesterol independent (Fig. 5C).

Next, we were interested in the effect of EGF on the colocalization of GPI-GFP with CTB. A clear colocalization at the

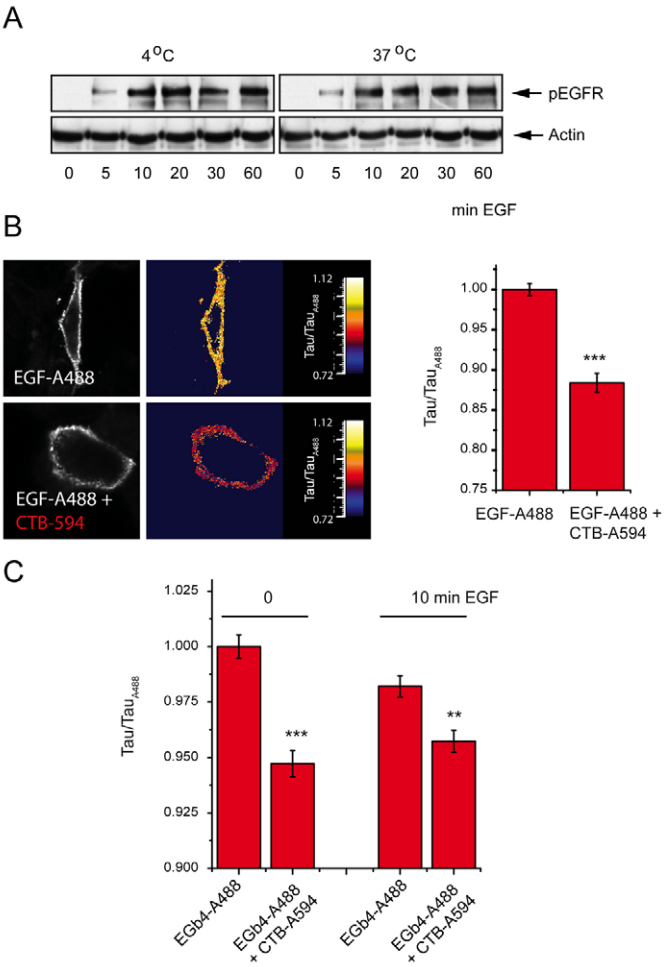

Fig. 4. EGF does not affect colocalization of EGFR with GM1 gangliosides (A) EGFR is activated at 4°C. HER14 cells were stimulated with 8 nM EGF for indicated times and temperatures. Cell lysates were prepared and analyzed by western blotting for the presence of phosphorylated tyrosine at position 1068 (pEGFR). Actin staining was used as loading control. (B) Colocalization of activated EGFR with GM1. HER14 cells were incubated on ice with 8 nM EGF-488 (donor) in the absence or presence of 1 μg/ml acceptor probe CTB-A594. Confocal images representing the distribution of EGF-A488 are shown in the left panel. The lifetime of EGF-A488 was determined as described in Materials and Methods and presented in false colors in the middle panel. Mean lifetime values ± s.e.m. (***P<0.0001) were determined and are presented in the histogram on the right. (C) EGF does not alter colocalization of EGFR and GM1. HER14 cells were incubated with 100 nM EGb4-A488 and 1 μg/ml CTB-A594 for 1 hour on ice. Cells were then either treated with 8 nM EGF for 10 minutes or left untreated. After fixation and embedding, lifetime values of EGb4-A488 were analyzed as described in Materials and Methods and are presented as mean lifetime values ± s.e.m. (**P<0.001, ***P<0.0001) in the histogram on the right.

nanoscale level was observed in resting cells (Fig. 3 and Fig. 5D). This was not significantly altered by a stimulation of the cell for 10 minutes with 8 nM EGF (Fig. 5D). To exclude a possible effect of the binding of CTB alone on the lifetime of GFP, we performed a lifetime analysis using CTB conjugated to biotin instead of the acceptor-probe Alexa-Fluor-594. No significant reduction in lifetime was observed, demonstrating the requirement for the fluorescent acceptor probe for this change in lifetime of the donor probe to occur (Fig. 5D). In summary, these data demonstrate that EGFR activation results in the induction of a cholesterol-independent

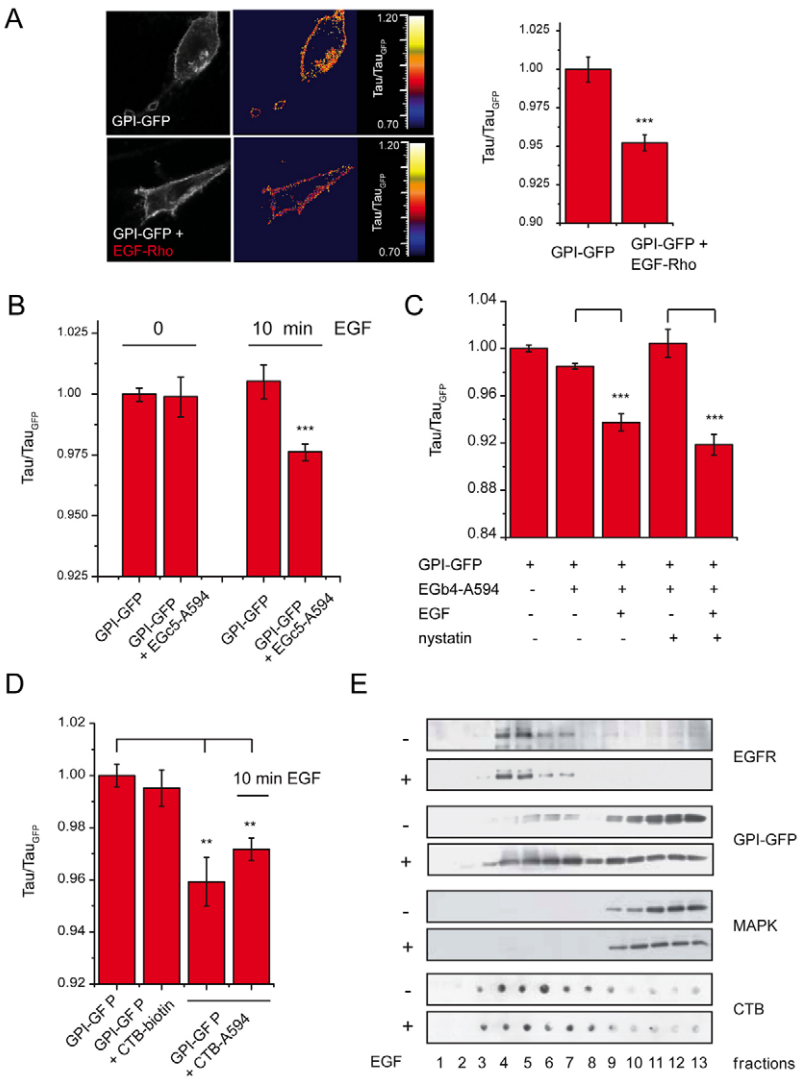

Fig. 5. EGF-induced colocalization of EGFR and GPI-GFP. (A) Colocalization active EGFR with GPI-GFP. HER14 cells expressing GPI-GFP were incubated for 1 hour on ice with 8 nM EGF-Rhodamine (EGF-Rho) for 60 minutes, or mock medium (without EGF-Rho). After fixation and embedding, the average lifetime values ± s.e.m. (***P<0.0001) of GPI-GFP were determined as described in Materials and Methods and are presented in the histogram on the right. (B) HER14 cells expressing GPI-GFP were incubated for 1 hour on ice with 100 nM EGc5-A594. Activation with 8 nM EGF was performed on ice for 10 minutes. After fixation and embedding, mean lifetime values ± s.e.m. (***P<0.0001) of GPI-GFP were determined as described in Materials and Methods and are presented in the histogram. (C) HER14 cells expressing GPI-GFP were pre-incubated or not with 5 μg/ml nystatin for 30 minutes at 37°C, for 1 hour on ice in the absence or presence of 100 nM CTB-A594, and stimulated or not for 10 minutes with 8 nM EGF. After fixation and embedding, average lifetime values ± s.e.m. (***P<0.0001) of GPI-GFP were determined as described in Materials and Methods and are presented in the histogram. (D) HER14 cells expressing GPI-GFP were incubated for 1 hour on ice in the absence or presence of 100 nM CTB-A594 or CTB-biotin as control. Activation with 8 nM EGF was performed on ice for 10 minutes. After fixation and embedding, mean lifetime values ± s.e.m. (**P<0.001) of GPI-GFP were determined as described in Materials and Methods and are presented in the histogram. (E) EGF induced the recruitment of GPI-GFP into the detergent-free lipid raft fraction. HER14 cells expressing GPI-GFP were stimulated or not with 8 nM EGF for 10 minutes, and detergent-free lipid raft fractions were isolated as described in Materials and Methods. Presence of EGFR, GPI-GFP and MAP kinase was analyzed by western blotting, presence of GM1 was determined using a dot-spot assay with CTB-HRP.

colocalization at the nanoscale level of EGFR with the lipid raft marker GPI-GFP.

We finally investigated whether the EGF-induced colocalization of GPI-GFP with EGFR could be supported also by fractionation studies. Detergent-free lipid raft fractions were purified and examined for the presence of EGFR, GPI-GFP and MAP kinase by western blotting, and GM1 by a dot-blot assay using CTB-HRP. EGF receptors, GPI-GFP and GM1 are all present in the lipid raft fraction, whereas MAP kinase is clearly absent. A clear enrichment of GPI-GFP was observed in the lipid raft fractions isolated from EGF-stimulated cells, whereas the distribution of EGFR, MAP kinase and GM1 remained unaffected (Fig. 5E). These data confirm the results that activation of the EGFR signaling pathway results in the coalescence of GM1–GPI-GFP and GM1-EGFR containing lipid rafts.

Discussion

In this study we have applied a ‘microspectroscopic’ approach to investigate the role of EGF signaling in the organization of lipid rafts. Nanometer-scale colocalization of the EGFR with putative lipid raft protein and glycolipid, and GPI-GFP and GM1, was investigated by FRET and analyzed by FLIM. For reliable interpretation of the FLIM results, the specific, non-agonistic and monovalent labeling of the EGFR is a prerequisite. This was achieved using nanobodies obtained from *Llama glama*. Labeling of GM1 was done with the pentavalent CTB subunit B. To exclude possible recruitment effects of this multimeric molecule, we have performed several control experiments. The absence of colocalization of CTB with TfR indicates that CTB does not colocalize with all plasma membrane receptors. In addition, the fact that the colocalization of GM1 with GPI-GFP was dependent upon cholesterol, makes it very unlikely that this colocalization is induced through the recruitment of GPI-GFP by the pentavalent CTB. To prevent the internalization of EGF-EGFR complexes without the use of inhibitors we have used the cold-induced internalization block. Under these conditions the EGFR was found to be stimulated by EGF in a similar way as at 37°C, which is in agreement with previous studies (McCune and Earp, 1989). In model membranes, however, effects of low temperature have been shown to stabilize lipid rafts (Baumgart et al., 2003). FRAP studies have previously shown that the lateral diffusion coefficient of the EGFR was reduced from 8.5×10^{-10} cm^2/second at 37°C to 2.8×10^{-10} cm^2/second at 5°C without any indication for a phase transition. This suggests that on the plasma membrane the low-

temperature conditions do not induce segregation of distinctive domains (Hillman and Schlessinger, 1982). Moreover, although the low-temperature condition completely inhibits the formation of clathrin-coated vesicles, the EGFR is still recruited to clathrin-coated pits (Puri et al., 2005). In conclusion, our control experiments seem to exclude side effects by the pentavalency of CTB and effects of the low temperature on the results.

Although we have obtained significant information about the occurrence of energy transfer between the EGFR-specific and the GM1-specific probes, the transfer efficiency appeared low. This could be explained by the relatively large distance between the EGFR-specific probes, i.e. the nanobodies and the GM1-probe. The crystal structure of the EGFR ectodomain suggests that, depending on the exact epitope recognized by the nanobody, the distance between the anti-EGFR nanobody and CTB can be more than 7 nm, which is larger than the Förster distance of the applied probes (Burgess et al., 2003; Ferguson et al., 2003). Although minor, the lifetime reduction due to FRET is highly significant. To exclude the possibility that the labeling of the EGFR or a conformational change of the receptor after activation does not influence the possibility of FRET, three different nanobodies were used that, according to their characteristics, bind to different sites of the EGFR ectodomain. In addition, we have also used fluorescent EGF to exclude any possible involvement of the nanobodies on the FRET analysis.

On a microscopic level, colocalization of the receptors for EGF and transferrin with GM1 and GPI-GFP was observed. At the nanometer scale level, our FRET analyses confirm the colocalization of GM1 with the EGFR but not with the TfR. The observed colocalization of EGFR with GM1 is in agreement with previous studies where electron microscopy was used (Puri et al., 2005; Ringerike et al., 2002). Similar results were obtained for HER2 (also known as ErbB2), another member of the EGFR family (Nagy et al., 2002). Sequestration of cholesterol did not affect the nanoscale colocalization of GM1 with the EGFR, suggesting that the colocalization of EGFR with GM1 is based upon a direct interaction between this ganglioside and the receptor. The gangliosides GM1 and GM3 were, indeed, shown to bind to the recombinant EGFR ectodomain purified from insect cells (Miljan et al., 2002). The interaction site appeared to be distinct from the ligand-binding site, implying that the cysteine-rich domain is responsible for this interaction. Interestingly, a mutational analysis demonstrated that the second cysteine-rich domain of the EGFR ectodomain is required for fractionation in the lipid raft fraction (Yamabhai and Anderson, 2002). NeuAc-lactose is essential for the direct interaction of gangliosides with the EGFR extracellular domain (Miljan et al., 2002). Whether sugar moieties on the EGFR extracellular domain are also involved in this interaction is currently unknown.

A consequence of the direct interaction between EGFR and gangliosides might be the formation of a lipid shell that surrounds the transmembrane domain of the EGFR, which could explain their fractionation into the lipid raft fraction (Fig. 5D). Furthermore, in this model, the molecular organization of GM1 as well as cholesterol might affect the conformation of the ectodomain of the receptor and, consequently, ligand binding. It might also have an influence on receptor dimerization or even predimer formation. A possible role for cholesterol on receptor clustering including pre-dimer formation has recently been demonstrated by fluorescence correlation spectrocopy in combination with fluorescent brightness analysis (Saffarian et al., 2007). Positive effects of GM1 levels on EGFR signaling were obtained by overexpression of GM1 generating enzymes, which resulted in improved EGF-dependent cell proliferation (Nishio et al., 2005). Similarly, addition of GD1a ganglioside has been shown to increase both the number of high-affinity receptors as well as to stimulate EGF-induced cell proliferation (Liu et al., 2004). However, inhibitory effects of gangliosides on EGFR signaling have been described for GM3. This suggests that different gangliosides in the EGFR-containing shell may have different effects on EGFR functioning. In conclusion, our data suggest the existence of a lipid shell around the EGFR, which is, at least, composed of gangliosides that have either a stimulative or inhibitory effect on EGFR functioning, depending on the type of prevailing ganglioside. The development of novel probes to detect the specific gangliosides is required to further substantiate this hypothesis.

The cholesterol-dependent colocalization of the two lipid raft markers GM1 and GPI-GFP is in agreement with previous studies (Kenworthy et al., 2000). We and others have previously shown that GPI-GFP exists in small cholesterol-dependent nanoclusters (Bader et al., 2007; Sharma et al., 2004). These anisotropy experiments suggest the existence of small clusters of three to four GPI-GFP molecules per microdomain. Our data suggest that gangliosides such as GM1 are also present in these clusters, as depicted in Fig. 6. The fact that the colocalization of GM1 with the EGFR was cholesterol-independent indicates the presence of two types of GM1-containing microdomain in the plasma membrane: a cholesterol-independent (GM1-EGFR) and a cholesterol-dependent microdomain (GM1–GPI-GFP).

The cholesterol-independent colocalization of the EGFR with GM1 seems to exclude an effect of cholesterol on EGFR functioning. However, sequestration of cholesterol in the plasma

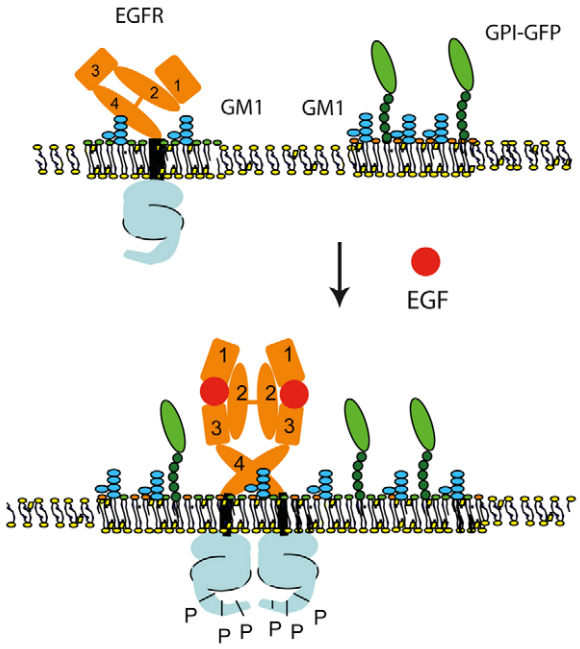

Fig. 6. Model showing the coalescence of different lipid rafts. In resting cells, GM1 forms a lipid shell that surrounds the EGFR by binding to the ectodomain, and colocalizes in a cholesterol-dependent manner with GPI-GFP. Stimulation of the cell with EGF results in the coalescence of these two different microdomains possibly leading to the formation of signaling platforms and the initiation of EGFR internalization.

membrane by nystatin or β-cyclodextrin was found to increase EGF-binding and ligand-independent activation of EGFR-kinase activity. Moreover, addition of cholesterol was found to inhibit EGFR signaling (Chen and Resh, 2002; Furuchi and Anderson, 1998; Ringerike et al., 2002). It is very well possible that the effect of cholesterol sequestration on EGFR functioning is indirect. Sequestration of cholesterol might lead to a disruption of the cholesterol-dependent lipid nanoclusters that contain GM1 and GPI-anchored proteins. Liberation of gangliosides from these types of raft might result in an increase in the direct interaction with the EGFR and, consequently, in more dramatic effects of GM1 on EGFR functioning. Addition of cholesterol to the cell, however, might have the adverse effect and induce the formation of larger cholesterol-dependent GM1–GPI-GFP rafts leading to a decrease in the availability of GM1 to bind the EGFR, and consequently to an inhibition of EGF signaling.

Upon activation of the EGFR, GPI-GFP was also found to colocalize at the nanometer scale with the EGFR. Similar results have previously been obtained with another GPI-linked protein, CD59 (Blagoev et al., 2003). This EGF-induced colocalization suggests the coalescence of the GM1-EGFR shells and the GM1–GPI-GFP nanoclusters into larger domains or rafts, a process schematically depicted in Fig. 6. Further proof for this interpretation was obtained by the isolation of detergent-free lipid raft fractions, which revealed an accumulation of GPI-GFP in the EGFR-containing lipid raft fraction after activation of the receptor. No change was observed in the already existing colocalization of GPI-GFP with GM1. The GPI-linked proteins do not have a direct interaction with the EGFR, indicating that EGFR-induced colocalization of GPI-linked proteins with the EGFR is probably the result of the fusion of the different lipid rafts in which these molecules are present (Fig. 6). The induced colocalization of EGFR with GPI-GFP was independent of cholesterol, suggesting that these novel structures are relatively stable. The coalescence can be regulated intracellularly by EGF-induced protein-protein interactions and/or by alterations in the membrane skeleton, which would explain the cholesterol independency. This mechanism would require a coupling between inner and outer leaflet domains, which has been recently described for the clustering of H-Ras by patching of GPI-anchored proteins (Eisenberg et al., 2006). Interestingly, EGF was also found to recruit other signaling proteins as Shc and Grb2 into the lipid raft fraction (Puri et al., 2005). The coalescence of the different types of nanocluster and the recruitment of other signaling molecules might therefore result in the formation of the so-called signaling platforms (Chen et al., 2006; Murakoshi et al., 2004; Simons and Toomre, 2000). Support for the signalling-platform hypothesis was recently described for GPI-anchored receptor clusters to which the signaling proteins phospholipase $C_{\gamma 2}$, phospholipase G_{α} and the non-receptor tyrosine kinase Lyn were recruited after initiation of signaling (Suzuki et al., 2007a; Suzuki et al., 2007b). These latter studies were performed using single-molecule imaging, emphasizing the need for different non-invasive biophysical methods for further analysis of membrane-bound signaling events.

An important negative-feedback control mechanism for the EGFR is the EGF-induced internalization of active EGFRs and subsequent routing to the lysosomes where activated receptors become degraded (Wiley, 2003). Clathrin-coated vesicles are generally accepted as the main entry portal for the EGFR. However, accumulating evidence suggests that also non-coated vesicles are involved in EGFR endocytosis, such as GM1-enriched vesicles (Puri et al., 2005), caveolae (Sigismund et al., 2005) and other pinocytotic vesicles (Orth et al., 2006). As such, the clustering of different shells and nanoclusters, which may lead to the formation of larger nanodomains as observed in our study, might represent an initial step for internalization. The local lipid composition in the clustered rafts might induce membrane curvature, which is essential for the internalization process (Hanzal-Bayer and Hancock, 2007). The question how this raft-mediated internalization of active EGFRs is regulated is the subject of our future research.

Materials and Methods

Materials

Mouse anti-EGFR and rabbit anti-EGFR antibodies were purchased from Santa-Cruz (Santa Cruz, CA) and Cell Signaling (Beverly, MA) respectively. Mouse anti-actin antibody was from MP Biomedicals (Aurora, OH) and mouse anti-GM130 and anti-phospho-tyrosine (clone PY20) antibodies were from BD Biosciences (Alphen aan de Rijn, The Netherlands). Mouse anti-GFP antibody was from Roche Diagnostics (Almere, The Netherlands), whereas anti-transferrin receptor (TfR) antibody was obtained from Invitrogen (Breda, The Netherlands). Human EGF was purchased from Oxford Biotechnologies (Oxfordshire, UK). Protein G-Sepharose 4B beads, BSA (Fraction V), Sepharose G25 medium beads, nystatin, filipin and Mowiol were from Sigma-Aldrich (Zwijndrecht, The Netherlands). Microcon YM-3 spin-columns were from Millipore (Billerica, MA). Molecular biology products and IPTG were from Fermentas GmbH (St Leon-Rot, Germany). Lipofectamine 2000, Zeocin and the fluorescent products EGF–Alexa-Fluor-488 (EGF-A488), EGF-tetramethylrhodamine, Transferrin–Alexa-Fluor-488, cholera toxin subunit B conjugated to Alexa-Fluor-594 (CTB-A594), biotin (CTB-biotin) or horseradish peroxidase (CTB-HRP), the Alexa-Fluor-488–TFP and Alexa-Fluor-594–NHS protein labeling kits were all from Invitrogen. Talon was purchased from BD Biosciences (Palo Alto, CA), and imidazole was obtained from Merck (Darmstadt, Germany). The GPI-GFP plasmid was kindly provided by Patrick Keller (Max Planck Institute of Molecular Cell Biology and Genetics, Dresden, Germany) and the plasmid expressing the TfR was a gift from Peter van der Sluijs (University Medical Center Utrecht, Utrecht, The Netherlands).

Cell culture and transfection

A431 (ATCC CRL-1555) and HER14 (mouse NIH 3T3 fibroblasts expressing human EGFR) cells were cultured in Dulbecco's modified Eagle's medium (DMEM) (Invitrogen) supplemented with 7.5% fetal bovine serum (v/v), 100 U/ml penicillin, 100 μg/ml streptomycin and 2 mM L-glutamine at 37°C in the presence of 5% CO_2 under a humidified atmosphere. For the immunoprecipitation and cell-activation experiments, cells were seeded in a 35-mm culture dish, and grown to subconfluency. Prior to stimulation, cells were maintained 12 hours under low serum (0.1% FCS) conditions. For transfection, cells were grown to 50% confluency and transfected with the indicated expression vectors by using Lipofectamine 2000 according to manufacturer's instructions (Invitrogen). Plasmid DNA was prepared using an endotoxin-free plasmid preparation kit (Machery-Nagel, Dueren, Germany). For FLIM experiments, the cells were used 48 hours post-transfection. To enrich cells expressing GPI-GFP, cells were sorted using a fluorescence-activated cell sorter. Cells pretreated with nystatin or filipin were incubated for 30 minutes at 37°C with DMEM supplemented with 5 μg/ml nystatin or 2.5 μg/ml filipin.

Nanobody selection, production and labeling

Synthesis of an immune phage antibody library was performed essentially as previously described (Roovers et al., 2007). In short, vesicles purified from EGFR-expressing A431 cell were injected into *Llama glama*. Four days after the last antigen injection, 150 ml of blood was collected and peripheral blood lymphocytes were collected by density-gradient centrifugation using Ficoll-Paque PLUS gradients (Amersham Biosciences, UK). Total RNA was extracted and transcribed into cDNA by using an oligo-dT primer and the SuperScript III First-Strand Synthesis system for RT-PCR (Invitrogen). The cDNA was subsequently treated with RNAse H to deplete residual RNA and then purified using the QIAquick PCR purification kit (Qiagen, Hilden, Germany). This cDNA was used as template to amplify the repertoire of gene segments encoding heavy chains of Ig with the use of a framework 1 (FR1)-specific primer and an oligo-dT primer. The resulting PCR fragments of 1.3 kb (heavy chain IgGs that lack the CH1 domain) and 1.6 kb (conventional IgGs) were separated by size on an agarose gel and the genes encoding the heavy-chain-only IgGs were purified. The full repertoire of PCR-amplified genes was digested with appropriate restriction enzymes and the resulting 400-500 bp fragments were ligated into a phagemid vector for display on a filamentous phage. This resulted in repertoires of 10^7-10^8 transformants each. Nanobodies specific for EGFR were subsequently selected by phage display. A431-derived membrane vesicles were coated onto a Maxisorp 96-well plate (Nunc, Denmark) during an overnight incubation at 4°C. Non-specific binding was prevented by blocking with 4% skimmed milk (Marvell) in PBS (MPBS) at room temperature (RT) for 30 minutes. Phages (~10^{10} colony-forming units), prepared from the immune library were panned for binding to immobilized EGFR

in 2% MPBS, 1% BSA containing suspended NIH 3T3 clone 2.2 cells (that do not express EGFR) for 90 minutes at room temperature. After extensive washing and elution with 100 mM triethylamine (TEA) for 10 minutes at room temperature, phages were neutralized and multiplied according to standard procedures. After selection, PCR products of single bacterial clones were analyzed by *Hin*fI restriction pattern analysis. The cDNAs of specific nanobody clones were re-cloned into pUR5850 allowing the expression of a triple-tagged protein (Myc, biotinylation and His6) in the periplasmic space of *E. coli*. Four hours after induction of nanobody production with IPTG, the bacteria were lysed in 8 M urea followed by purification of the nanobody with Talon beads according to the manufacturer's instructions. Purified protein was dialyzed extensively against PBS, and checked for purity on a Coomassie-Blue-stained SDS-polyacrylamid gel. Micropore spin columns were used to concentrate the pure protein to a final concentration of 2-5 mg/ml. Labeling of nanobodies with Alexa-Fluor-488 or -594 was performed as recommended by the manufacturer. In short, 15 μg of nanobody was incubated with 3-30 μg of DMSO-dissolved mono-reactive Alexa-Fluor dye for 1 hour at room temperature in the dark. Labeled nanobody was separated from non-reacting dye using a 1 ml Sephadex G25 column and dialyzed against PBS. Labeling efficiency was determined with a Nanodrop spectrophotometer (Nanodrop Technologies, Wilmington, Delaware), and came on average to 1.5 Alexa-Fluor label per nanobody. Final concentration of the fluorescent nanobodies used for cell labeling varied between 50 and 100 nM.

An ELISA assay was performed to determine the competition between EGF and nanobodies to bind the EGFR as previously described (Roovers et al., 2007). In short, A431-derived membrane vesicles were immobilized overnight at 4°C in 96-well plates (Maxisorp, Costar, Corning) at 5 μg/ml of protein. The next day, plates were washed twice with PBS containing 0.05% Tween-20 (v/v) and subsequently blocked with PBS containing 1% casein (w/v) for 1 hour at room temperature. Serial dilutions of nanobodies (200 nM to 10 pM) were made in PBS/1% casein (w/v), biotinylated EGF (Peprotech, New York, NY) was added to 8 ng/ml (1.3 nM) and the mixes were incubated in vesicle-coated wells for 1 hour at room temperature while shaking. Maximal binding was determined by addition of a non-relevant (anti-GST) nanobody and background staining by the omission of biotinylated EGF. Wells were washed three times with PBS/0.05% Tween-20 (v/v) and receptor-bound biotinylated EGF was detected with a streptavidin-peroxydase conjugate [Sigma-Aldrich, Zwijndrecht, The Netherlands; 1:5000 in PBS/1% (w/v) casein]. After washing, wells were stained using O-phenylenediamine (OPD, MP Biomedicals, Illkirch, France) and the reaction was stopped by the addition of 1 M H_2SO_4. The OD was read at 490 nm in a 96-well ELISA reader.

Immunoprecipitation

Immunoprecipitation experiments were principally performed as described previously (Klapisz et al., 2002). HER14 cells were grown in 35-mm dishes until 70% confluency and lysed in ice-cold 300 μl lysis buffer (1% Triton X-100, 150 mM NaCl, 20 mM Tris-HCl pH 7.4) supplemented with complete protease inhibitor cocktail (Roche), 10 mM NaF, and 1 mM $NaVO_4$. The lysate was passed through a 23G needle three times and centrifuged at 13,000 ***g*** for 5 minutes. Talon beads (20 μl), preloaded with 10 μg of the indicated nanobodies for 1 hour were incubated with the lysates for 1 hour at 4°C. The beads were washed extensively with lysis buffer and resuspended in 40 μl sample buffer. Precipitated proteins were size-separated on 8% (w/v) SDS-PAGE and transferred onto PVDF membrane. EGFR was detected using anti-EGFR (Santa Cruz Biotechnology) and horseradish peroxidase (HRP-conjugated anti-rabbit IgG (Jackson ImmunoResearch Laboratories), followed by signal detection using ECL (Du Pont NEN).

Immunofluorescent labeling

Cells (~6×10^4) were seeded on 18-mm glass coverslips and grown until 20% confluency. Medium was replaced by ice-cold binding medium [DMEM-Hepes (pH 7.8) supplemented with 1% BSA], and the cells were placed on ice. Cells were subsequently incubated with fluorescent EGF (8 nM), CTB (1 μg/ml), transferrin (20 μg/ml) or different nanobodies (50-100 nM) in binding medium for 1 hour on ice. Cells preincubated with nystatin or filipin were maintained in binding medium supplemented with the labeling reagents. Cells were washed with binding medium, fixed with, initially, ice-cold 4% formaldehyde, and quenched with 50 mM glycine. Coverslips were finally embedded in Mowiol and stored at –20°C until further use. Wide-field microscopy was performed on an Olympus AX70 microscope equipped with a Nikon CCD camera (DXM1200) using a 60× oil-immersion objective (NA 1.25/ PlanFl). Confocal microscopy for Fig. 1C was done on a Zeiss LSM 510 microscope equipped with a 63× water-immersion objective (NA 1.2/C-apochromat).

Fluorescence lifetime imaging measurement (FLIM)

A Nikon PCM 2000 confocal scanning laser microscope (CSLM) was equipped with a fluorescence lifetime imaging module (LiMO, Nikon Instruments, Badhoevedorp, The Netherlands) (de Grauw and Gerritsen, 2001), which captures four images representing the total fluorescent intensity in four consecutive time gates of approximately 2 nanoseconds each. The excitation light was provided by a frequency-doubled picosecond-pulsed Ti-Sa laser (Tsunami, Spectra Physics); a pulse picker was used to reduce the repetition rate to 8.2 MHz. 460-nm pulses were transferred to the confocal microscope using a single-mode optical fiber. For imaging, a NA 1.20/40× water-immersion objective (Plan Apo, Nikon) and the medium-sized pinhole were used. The fluorescence emission was filtered (515/30 emission filter) and collected with a fiber-coupled PMT (Hamamatsu H7422P-40) that was connected to a pre-amplifier and the LiMo unit. To set the time, offset of opening of the first gate of the LiMo with respect to the excitation pulse, a solution of Rose Bengal (lifetime 70 picoseconds), was used in such a way that the first gate opened after 90% of the fluorescence was emitted. The widths of the time gates were calibrated using a continuous source of white light; correction factors were introduced to ensure that intensity was equal in all gates. The four-gate intensity decays recorded for each pixel were fitted with a monoexponential decay using the LiMO software, meaning that also for probes with multiexponential decays, one single average lifetime is observed. Lifetimes described in this study should therefore be considered as average lifetimes.

Analysis of FRET/FLIM data

Confocal FRET/FLIM microscopy was used to make lifetime images in an equatorial plane through the cell (supplementary material Fig. S5A,B). Subsequently, intensity thresholding was performed to remove background- (glass) and auto-fluorescence (supplementary material Fig. S5C,D). The fluorescence lifetimes of pixels above threshold (at least 1000 per cell) were plotted in a histogram that was fitted with a Gaussian function (using Origin, Origin Corporation, Northampton, MA) to determine the average lifetime (supplementary material Fig. S5E). To rule out the effects of cell-to-cell variation in FRET efficiency, the lifetimes of at least five cells were determined and a Student's *t*-test was performed to determine the statistical significances (supplementary material Fig. S5F). Fluorescent lifetimes were normalized against the lifetime for donor-only situation. For one cell, normalized fluorescence lifetime values are presented in a false-color image; histograms show the normalized average donor lifetime $\tau/\tau_{donor} \pm$ standard error of the mean (± s.e.m.) for $n \geq 5$ cells per measurement.

Purification of detergent-free lipid raft fractions

The procedure for detergent-free cell fractionation and flotation was modified from MacDonald and Pike (Macdonald and Pike, 2005). Briefly, two 100-mm dishes with HER14 cells expressing GPI-GFP were grown to 80% confluency. Cells were grown in serum-free medium for 16 hours. Prior to the fractionation, medium was replaced by ice-cold serum-free DMEM with Hepes buffer (pH 7.2), and cells were either stimulated at 4°C with 8 nM EGF for 10 minutes or left untreated. After washing twice with ice-cold PBS, cells were scraped in base buffer (20 mM Tris-HCl, 250 mM sucrose, pH 7.8) supplemented with 1 mM $MgCl_2$ and 1 mM $CaCl_2$. After pelleting the cells by centrifugation at 250 ***g***, they were resuspended in base buffer supplemented with Complete protease inhibitor cocktail, 1 mM $MgCl_2$ and 1 mM $CaCl_2$. The cells were lysed by passing through a 23G needle for 20 times. After centrifugation at 1000 ***g*** for 10 minutes, the post-nuclear supernatant was harvested. The remaining pellet was resuspended in base buffer with Complete protease inhibitor cocktail and cations, passed through the needle 20 times again, followed by centrifugation. The second supernatant was combined with the first. Optiprep was added to a final concentration of 25%. Subsequently, a 0-20% Optiprep step-gradient with 5% intervals was layered on top of this lysate, and centrifuged at 52,000 ***g*** for 90 minutes using a Beckmann SW41Ti rotor. A total of 12 fractions of 1 ml each were collected from top to bottom of the gradient. To concentrate proteins, fractions were concentrated on Microcon columns (MWCO 3 kDa) until a final volume of 40 μl was reached. Proteins in the different fractions were size-separated on a 8% SDS-PAGE, and analyzed by western blotting. Detection of GM1 was performed using a dot-spot assay as described by Puri et al., using CTB conjugated to HRP as ligand (Puri et al., 2005).

We thank Edward Dolk, Hein Sprong and Gerrit van Meer for helpful discussions and reading of the manuscript, and Ger J. A. Arkestein for his help with the FACS sorting. This research was supported in part by the Dutch Organization for Scientific Research [NWO-ALW, Molecule to Cell (MtC) program] (E.G.H. and A.N.B.). M.O.R. was supported by a personal stipend from the Finnish Cultural Foundation.

References

Bader, A. N., Hofman, E. G., van Bergen en Henegouwen, P. M. P. and Gerritsen, H. C. (2007). Imaging of protein cluster size by means of confocal time-gated fluorescence anisotropy microscopy. *Opt. Express* **15**, 6934-6945.

Baumgart, T., Hess, S. T. and Webb, W. W. (2003). Imaging coexisting fluid domains in biomembrane models coupling curvature and line tension. *Nature* **425**, 821-824.

Blagoev, B., Kratchmarova, I., Ong, S. E., Nielsen, M., Foster, L. J. and Mann, M. (2003). A proteomics strategy to elucidate functional protein-protein interactions applied to EGF signaling. *Nat. Biotechnol.* **21**, 315-318.

Bremer, E. G., Hakomori, S., Bowen-Pope, D. F., Raines, E. and Ross, R. (1984). Ganglioside-mediated modulation of cell growth, growth factor binding, and receptor phosphorylation. *J. Biol. Chem.* **259**, 6818-6825.

Burgess, A. W., Cho, H. S., Eigenbrot, C., Ferguson, K. M., Garrett, T. P., Leahy, D. J., Lemmon, M. A., Sliwkowski, M. X., Ward, C. W. and Yokoyama, S. (2003). An open-and-shut case? Recent insights into the activation of EGF/ErbB receptors. *Mol. Cell* **12**, 541-552.

Chen, X. and Resh, M. D. (2002). Cholesterol depletion from the plasma membrane triggers ligand-independent activation of the epidermal growth factor receptor. *J. Biol. Chem.* **277**, 49631-49637.

Chen, Y., Thelin, W. R., Yang, B., Milgram, S. L. and Jacobson, K. (2006). Transient anchorage of cross-linked glycosyl-phosphatidylinositol-anchored proteins depends on cholesterol, Src family kinases, caveolin, and phosphoinositides. *J. Cell Biol.* **175**, 169-178.

Conrath, K. E., Wernery, U., Muyldermans, S. and Nguyen, V. K. (2003). Emergence and evolution of functional heavy-chain antibodies in Camelidae. *Dev. Comp. Immunol.* **27**, 87-103.

Dawson, J. P., Bu, Z. and Lemmon, M. A. (2007). Ligand-induced structural transitions in ErbB receptor extracellular domains. *Structure* **15**, 942-954.

de Grauw, C. J. and Gerritsen, H. C. (2001). Multiple time-gate module for fluorescence lifetime imaging. *Appl. Spectrosc.* **55**, 670-678.

den Hartigh, J. C., van Bergen en Henegouwen, P. M. P., Boonstra, J. and Verkleij, A. J. (1993). Cholesterol and phosphoinositides increase affinity of the epidermal growth factor receptor. *Biochim. Biophys. Acta* **1148**, 249-256.

Eisenberg, S., Shvartsman, D. E., Ehrlich, M. and Henis, Y. I. (2006). Clustering of raft-associated proteins in the external membrane leaflet modulates internal leaflet H-ras diffusion and signaling. *Mol. Cell. Biol.* **26**, 7190-7200.

Ferguson, K. M., Berger, M. B., Mendrola, J. M., Cho, H. S., Leahy, D. J. and Lemmon, M. A. (2003). EGF activates its receptor by removing interactions that autoinhibit ectodomain dimerization. *Mol. Cell* **11**, 507-517.

Foster, L. J., De Hoog, C. L. and Mann, M. (2003). Unbiased quantitative proteomics of lipid rafts reveals high specificity for signaling factors. *Proc. Natl. Acad. Sci. USA* **100**, 5813-5818.

Furuchi, T. and Anderson, R. G. (1998). Cholesterol depletion of caveolae causes hyperactivation of extracellular signal-related kinase (ERK). *J. Biol. Chem.* **273**, 21099-21104.

Hanzal-Bayer, M. F. and Hancock, J. F. (2007). Lipid rafts and membrane traffic. *FEBS Lett*. **581**, 2098-2104.

Harder, T., Scheiffele, P., Verkade, P. and Simons, K. (1998). Lipid domain structure of the plasma membrane revealed by patching of membrane components. *J. Cell Biol.* **141**, 929-942.

Hillman, G. M. and Schlessinger, J. (1982). Lateral diffusion of epidermal growth factor complexed to its surface receptors does not account for the thermal sensitivity of patch formation and endocytosis. *Biochemistry* **21**, 1667-1672.

Jacobson, K., Mouritsen, O. G. and Anderson, R. G. (2007). Lipid rafts: at a crossroad between cell biology and physics. *Nat. Cell Biol.* **9**, 7-14.

Jares-Erijman, E. A. and Jovin, T. M. (2006). Imaging molecular interactions in living cells by FRET microscopy. *Curr. Opin. Chem. Biol.* **10**, 409-416.

Jorissen, R. N., Walker, F., Pouliot, N., Garrett, T. P., Ward, C. W. and Burgess, A. W. (2003). Epidermal growth factor receptor: mechanisms of activation and signalling. *Exp. Cell Res.* **284**, 31-53.

Kenworthy, A. K., Petranova, N. and Edidin, M. (2000). High-resolution FRET microscopy of cholera toxin B-subunit and GPI-anchored proteins in cell plasma membranes. *Mol. Biol. Cell* **11**, 1645-1655.

Klapisz, E., Sorokina, I., Lemeer, S., Pijnenburg, M., Verkleij, A. J. and van Bergen en Henegouwen, P. M. P. (2002). A ubiquitin-interacting motif (UIM) is essential for Eps15 and Eps15R ubiquitination. *J. Biol. Chem.* **277**, 30746-30753.

Kusumi, A., Koyama-Honda, I. and Suzuki, K. (2004). Molecular dynamics and interactions for creation of stimulation-induced stabilized rafts from small unstable steady-state rafts. *Traffic* **5**, 213-230.

Lagerholm, B. C., Weinreb, G. E., Jacobson, K. and Thompson, N. L. (2005). Detecting microdomains in intact cell membranes. *Annu. Rev. Phys. Chem.* **56**, 309-336.

Lambert, S., Vind-Kezunovic, D., Karvinen, S. and Gniadecki, R. (2006). Ligand-independent activation of the EGFR by lipid raft disruption. *J. Invest. Dermatol.* **126**, 954-962.

Li, R., Liu, Y. and Ladisch, S. (2001). Enhancement of epidermal growth factor signaling and activation of SRC kinase by gangliosides. *J. Biol. Chem.* **276**, 42782-42792.

Lichtenberg, D., Goni, F. M. and Heerklotz, H. (2005). Detergent-resistant membranes should not be identified with membrane rafts. *Trends Biochem. Sci.* **30**, 430-436.

Liu, Y., Li, R. and Ladisch, S. (2004). Exogenous ganglioside GD1a enhances epidermal growth factor receptor binding and dimerization. *J. Biol. Chem.* **279**, 36481-36489.

Macdonald, J. L. and Pike, L. J. (2005). A simplified method for the preparation of detergent-free lipid rafts. *J. Lipid Res.* **46**, 1061-1067.

Mayor, S. and Rao, M. (2004). Rafts: scale-dependent, active lipid organization at the cell surface. *Traffic* **5**, 231-240.

McCune, B. K. and Earp, H. S. (1989). The epidermal growth factor receptor tyrosine kinase in liver epithelial cells. The effect of ligand-dependent changes in cellular location. *J. Biol. Chem.* **264**, 15501-15507.

Miljan, E. A. and Bremer, E. G. (2002). Regulation of growth factor receptors by gangliosides. *Sci. STKE* **2002**, RE15.

Miljan, E. A., Meuillet, E. J., Mania-Farnell, B., George, D., Yamamoto, H., Simon, H. G. and Bremer, E. G. (2002). Interaction of the extracellular domain of the epidermal growth factor receptor with gangliosides. *J. Biol. Chem.* **277**, 10108-10113.

Mineo, C., James, G. L., Smart, E. J. and Anderson, R. G. (1996). Localization of epidermal growth factor-stimulated Ras/Raf-1 interaction to caveolae membrane. *J. Biol. Chem.* **271**, 11930-11935.

Murakoshi, H., Iino, R., Kobayashi, T., Fujiwara, T., Ohshima, C., Yoshimura, A. and Kusumi, A. (2004). Single-molecule imaging analysis of Ras activation in living cells. *Proc. Natl. Acad. Sci. USA* **101**, 7317-7322.

Nagy, P., Vereb, G., Sebestyen, Z., Horvath, G., Lockett, S. J., Damjanovich, S., Park, J. W., Jovin, T. M. and Szollosi, J. (2002). Lipid rafts and the local density of ErbB proteins influence the biological role of homo- and heteroassociations of ErbB2. *J. Cell. Sci.* **115**, 4251-4262.

Nishio, M., Tajima, O., Furukawa, K. and Urano, T. (2005). Over-expression of GM1 enhances cell proliferation with epidermal growth factor without affecting the receptor localization in the microdomain in PC12 cells. *Int. J. Oncol.* **26**, 191-199.

Orr, G., Hu, D., Ozcelik, S., Opresko, L. K., Wiley, H. S. and Colson, S. D. (2005). Cholesterol dictates the freedom of EGF receptors and HER2 in the plane of the membrane. *Biophys. J.* **89**, 1362-1373.

Orth, J. D., Krueger, E. W., Weller, S. G. and McNiven, M. A. (2006). A novel endocytic mechanism of epidermal growth factor receptor sequestration and internalization. *Cancer Res.* **66**, 3603-3610.

Pike, L. J. (2004). Lipid rafts: heterogeneity on the high seas. *Biochem. J.* **378**, 281-292.

Pike, L. J. (2005). Growth factor receptors, lipid rafts and caveolae: an evolving story. *Biochim. Biophys. Acta* **1746**, 260-273.

Pike, L. J. and Casey, L. (2002). Cholesterol levels modulate EGF receptor-mediated signaling by altering receptor function and trafficking. *Biochemistry* **41**, 10315-10322.

Puri, C., Tosoni, D., Comai, R., Rabellino, A., Segat, D., Caneva, F., Luzzi, P., Di Fiore, P. P. and Tacchetti, C. (2005). Relationships between EGFR signaling-competent and endocytosis-competent membrane microdomains. *Mol. Biol. Cell* **16**, 2704-2718.

Rao, M. and Mayor, S. (2005). Use of Forster's resonance energy transfer microscopy to study lipid rafts. *Biochim. Biophys. Acta* **1746**, 221-233.

Ringerike, T., Blystad, F. D., Levy, F. O., Madshus, I. H. and Stang, E. (2002). Cholesterol is important in control of EGF receptor kinase activity but EGF receptors are not concentrated in caveolae. *J. Cell. Sci.* **115**, 1331-1340.

Roepstorff, K., Thomsen, P., Sandvig, K. and van Deurs, B. (2002). Sequestration of epidermal growth factor receptors in non-caveolar lipid rafts inhibits ligand binding. *J. Biol. Chem.* **277**, 18954-18960.

Roovers, R. C., Laeremans, T., Huang, L., De Taeye, S., Verkleij, A. J., Revets, H., de Haard, H. J. and van Bergen en Henegouwen, P. M. P. (2007). Efficient inhibition of EGFR signaling and of tumour growth by antagonistic anti-EFGR nanobodies. *Cancer Immunol. Immunother.* **56**, 303-317.

Saffarian, S., Li, Y., Elson, E. L. and Pike, L. J. (2007). Oligomerization of the EGF receptor investigated by live cell fluorescence intensity distribution analysis. *Biophys. J.* **93**, 1021-1031.

Sharma, P., Varma, R., Sarasij, R. C., Ira Gousset, K., Krishnamoorthy, G., Rao, M. and Mayor, S. (2004). Nanoscale organization of multiple GPI-anchored proteins in living cell membranes. *Cell* **116**, 577-589.

Sigismund, S., Woelk, T., Puri, C., Maspero, E., Tacchetti, C., Transidico, P., Di Fiore, P. P. and Polo, S. (2005). Clathrin-independent endocytosis of ubiquitinated cargos. *Proc. Natl. Acad. Sci. USA* **102**, 2760-2765.

Simons, K. and Toomre, D. (2000). Lipid rafts and signal transduction. *Nat. Rev. Mol. Cell. Biol.* **1**, 31-39.

Suzuki, K. G., Fujiwara, T. K., Edidin, M. and Kusumi, A. (2007a). Dynamic recruitment of phospholipase C gamma at transiently immobilized GPI-anchored receptor clusters induces IP3-Ca2+ signaling: single-molecule tracking study 2. *J. Cell Biol.* **177**, 731-742.

Suzuki, K. G., Fujiwara, T. K., Sanematsu, F., Iino, R., Edidin, M. and Kusumi, A. (2007b). GPI-anchored receptor clusters transiently recruit Lyn and G alpha for temporary cluster immobilization and Lyn activation: single-molecule tracking study 1. *J. Cell Biol.* **177**, 717-730.

Wiley, H. S. (2003). Trafficking of the ErbB receptors and its influence on signaling. *Exp. Cell Res.* **284**, 78-88.

Yamabhai, M. and Anderson, R. G. (2002). Second cysteine-rich region of epidermal growth factor receptor contains targeting information for caveolae/rafts. *J. Biol. Chem.* **277**, 24843-24846.

Zhang, R. G., Westbrook, M. L., Westbrook, E. M., Scott, D. L., Otwinowski, Z., Maulik, P. R., Reed, R. A. and Shipley, G. G. (1995). The 2.4 A crystal structure of cholera toxin B subunit pentamer: choleragenoid. *J. Mol. Biol.* **251**, 550-562.

Zurita, A. R., Maccioni, H. J. and Daniotti, J. L. (2001). Modulation of epidermal growth factor receptor phosphorylation by endogenously expressed gangliosides. *Biochem. J.* **355**, 465-472.